We are IntechOpen,
the world's leading publisher of
Open Access books
Built by scientists, for scientists

6,900
Open access books available

185,000
International authors and editors

200M
Downloads

Our authors are among the

154
Countries delivered to

TOP 1%
most cited scientists

12.2%
Contributors from top 500 universities

BOOK CITATION INDEX
CLARIVATE ANALYTICS
INDEXED

WEB OF SCIENCE™

Selection of our books indexed in the Book Citation Index
in Web of Science™ Core Collection (BKCI)

Interested in publishing with us?
Contact book.department@intechopen.com

Numbers displayed above are based on latest data collected.
For more information visit www.intechopen.com

Zinc-Tin-Oxide-Based Porous Ceramics: Structure, Preparation and Properties

Tamara Ivetić

Additional information is available at the end of the chapter

Abstract

Zinc-tin-oxide-based ceramics have been extensively investigated especially regarding the synthesis of zinc stannate (Zn_2SnO_4), a spinel structure ternary compound with a wide range of possible applications. Among all of those, the best-known use of this material is in the combustion gas and moisture sensors. This chapter presents the research results review on the structure, morphology, and properties of mechanochemically synthesized Zn_2SnO_4 ceramics with large open porosity, as well as the results obtained during its solid-state processing optimization. Also shown is the review of the results obtained in the study of the influence of addition of the small amounts of bismuth oxide (Bi_2O_3) on the obtained Zn_2SnO_4 structure, microstructure, and electrical properties, as it provides the condition for the liquid phase sintering and creates a new dynamics in the zinc-tin-oxide reaction sintering process.

Keywords: $ZnO\text{-}SnO_2$ ceramics, spinels, zinc stannate, mechanical activation, sintering

1. Introduction

Zinc stannate is a non-toxic transparent n-type semiconducting oxide material whose electrical conductivity is sensitive to the changes of oxygen stoichiometry and environmental atmosphere, so it is mostly known for its gas-sensing (detection of combustion gases, CO, H_2, NO, NO_2, and moisture) applications [1–3]. However, the unique electrical and optical properties of the zinc stannate, which has been manufactured so far in different forms (thin and thick films, polycrystalline powders, composite and porous sintered ceramics) [4–7], makes it a suitable material for the various other applications as well (as functional coatings, flat panel displays, thin film solar cells, windows coatings, transparent conducting electrodes, as anode material in Li-ion batteries, as various photoelectrical devices, in photocatalysis) [8–20]. Zinc stannate is a spinel compound with a general formula Zn_2SnO_4 and a band gap of 3.6 eV. The spinel

Zn_2SnO_4 in the bulk form is stable in the inverse spinel structure, with a face-centered cubic unit cell (space group Fd3m), where Zn^{2+} occupy the 8a sites, and both Zn^{2+} and Sn^{4+} cations occupy the 16d sites, while O is placed in the 32e sites. Its unit cell parameter has a value of a = 8.6574 Å (JCPDS PDF 24-1470). The spinel-type structures can have big cation disorders in the crystal lattice and certain nonstoichiometry. Nevertheless, the disorders in spinels are not conventional so there is no change in the symmetry. The most general spinel formula is AB_2O_4, where A is two valent or four valent metal ions, and B are two valent or tree valent metal ions. To this day, there have been synthesized over 200 different types of spinel oxide compounds. Some spinel compounds are known to have the characteristic sensor and catalytic properties, like Zn_2SnO_4, and exhibit complex disordering phenomena related to the redistribution of cations over (B) and [A] sublattices in their structure. The partly inverse spinels like Zn_2SnO_4 have four valent ions on octahedral positions [A] and two valent ions in some ration distributed over tetrahedral (B) and octahedral coordination [A]. The zinc stannate compound may then be presented as $(Zn^{2+})[Sn^{4+}Zn^{2+}]O_4$ to emphasize the site occupancy at the atomic level.

The previous solid-state synthesis investigations established that complete Zn_2SnO_4 formation needs prolonged mechanical activation of the starting reaction precursors (ZnO and SnO_2 powders) and considerable high temperature of sintering (in the range from 1000 to 1280°C). The solid-state chemical reaction between the ZnO and SnO_2 starts relatively slow at 1000°C while the monophase polycrystalline zinc stannate is formed at 1280°C.

2. Mechanochemical activation and consolidation of ZnO-SnO$_2$ powder system

Finding optimal conditions of mechanochemical activation is the first and foremost important processing step for obtaining the right texture, particle size distribution and chemical reactivity of the starting powders in the solid-state synthesis of the polycrystalline Zn_2SnO_4 ceramics and the achievement of the wide range of its applications [21]. The mechanochemical activation consists of several processes that are usually divided into four stages: the material destruction, new surface formation, fine grinding and transformation to a completely different material structure. The optimal powder processing is a way to lower the sintering temperature necessary in the further steps of the ceramics production, which is very important fact from the stand point of the cost-effectiveness. When the starting powders of zinc oxide and tin oxide in the 2:1 molar ratio (ZnO:SnO$_2$ = 2:1) are mechanically activated in a planetary ball mill (Fritsch Pulverisette) in time intervals 0–160 min (with 320 rpm, ball to powder mass ratio of 40:1, in zirconium grinding media of a 500 ml vial and 10 mm diameter balls) the two stages of the grinding process occurs (**Figure 1**). The investigated samples were marked further in the text as ZSO-00, ZSO-10, ZSO-40, ZSO-80, and ZSO-160, and these marks are related to the not-activated, 10, 40, 80, and 160 min activated 2ZnO-SnO$_2$ powder mixtures, respectively. The first stage, up to 10 min of mechanical activation, is the increase in the powders specific surface area (S_{BET}, calculated by BET method from the linear part of N_2 adsorption isotherms [21–23]) which is related to the breaking of the powder particles and formation of the new surfaces (**Figure 2a** and **b**). The second stage brings the cold-welding and chemical reaction between the starting precursors (ZnO and SnO_2 powders),
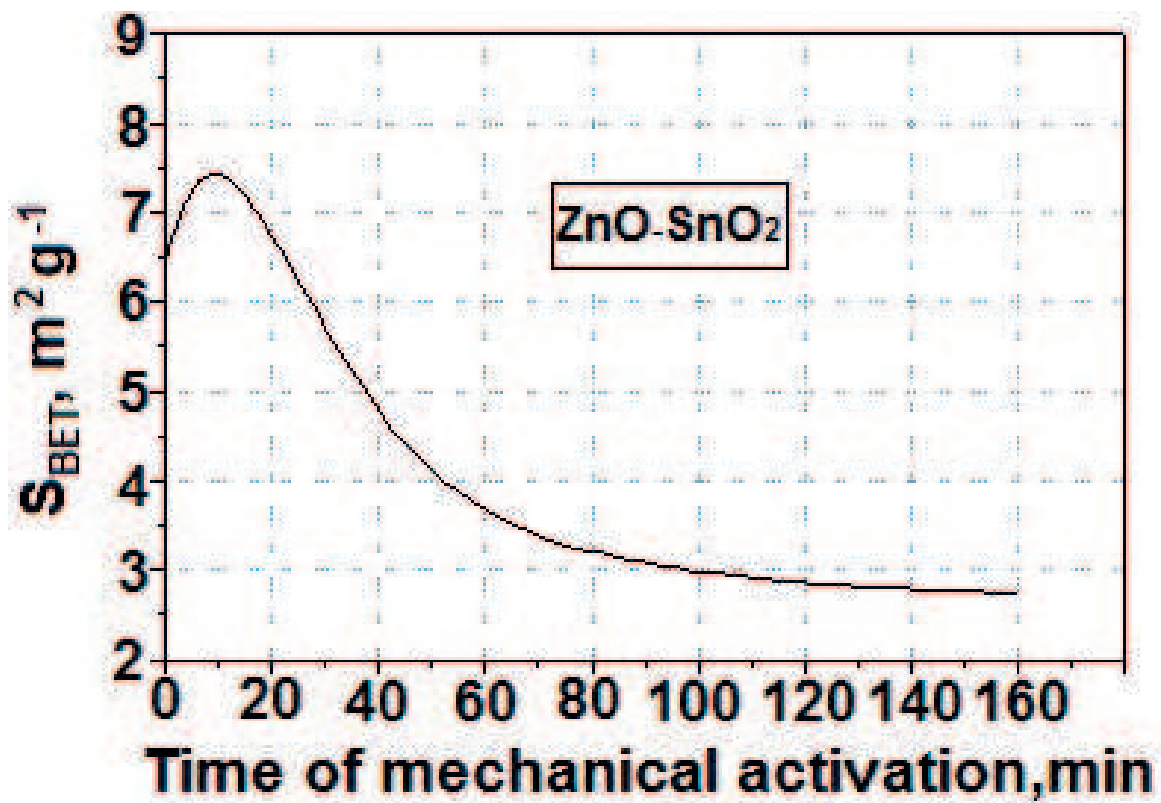
Figure 1. The specific surface area vs. the time of mechanical activation for the ZnO-SnO$_2$ powder system.
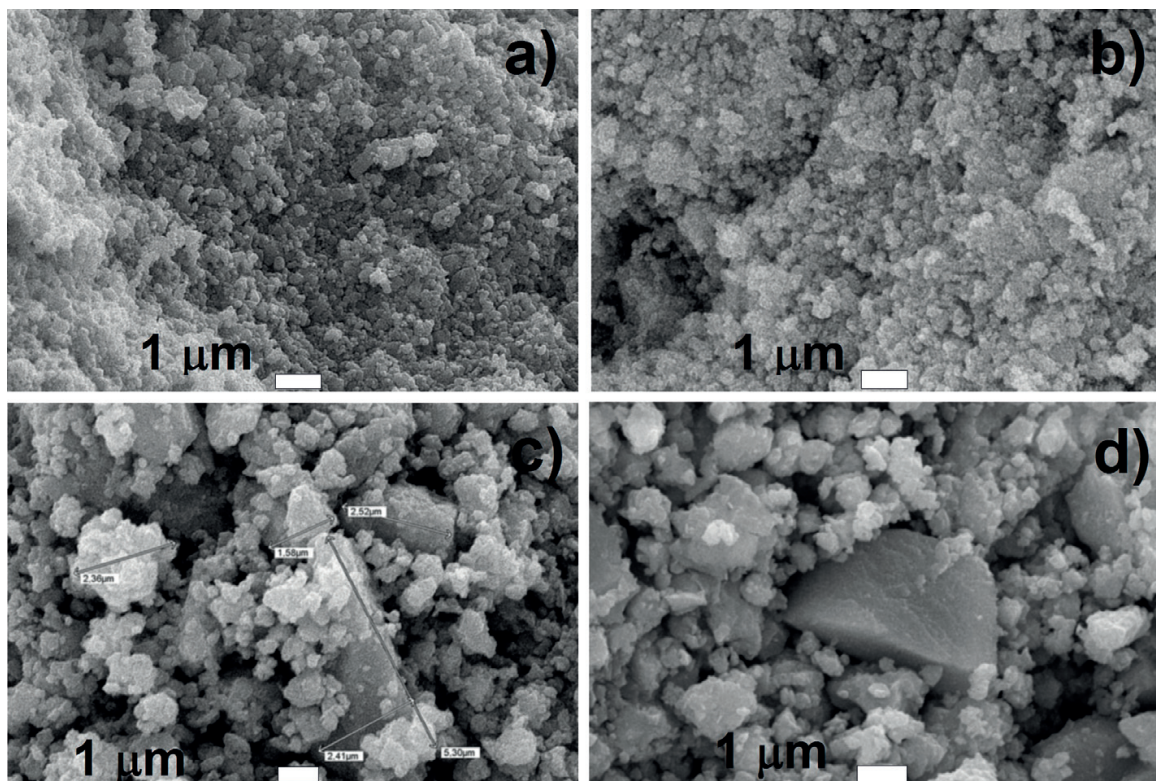

Figure 2. SEM micrographs of ZnO-SnO$_2$ powder mixtures activated, (a) 0, (b) 10, (c) 40, and (d) 80 min.

a formation of a new phase and a decrease in the S_{BET} (**Figure 2c** and **d**). The first sign of the spinel zinc stannate formation was noticed after 40 min of mechanical activation (results obtained by X-ray diffraction, XRD [21]). By increasing the activation time the intensities of the XRD peaks of the starting phases ZnO and SnO_2, become lower while XRD peaks of the spinel Zn_2SnO_4 phase dominates. After 160 min of mechanical activation, the Zn_2SnO_4 becomes a major phase in the system. Together with the progression of the mechanochemical reaction and formation of the zinc stannate spinel a secondary agglomeration occurs as well, which contributes mostly to a continuous decrease of S_{BET} during the second stage of the grinding process (**Figure 2c** and **d**). The microstructure of the starting ZnO and SnO_2 powder mixture characterizes in the homogeneously distributed particles of two kinds, the smaller ones with a spherical shape that belongs to ZnO and the longer ones with a polygonal shape, which belongs to the SnO_2. After 10 min of activation, there is a noticeable decrease in a number of the spherical particles because ZnO is more than six times softer material than SnO_2 (microhardness of ZnO and SnO_2 is 1.5 and 10 GPa, respectively) so firstly the drastic changes induced by mechanical activation addresses the ZnO (**Figure 2**).

The shape of the adsorption isotherms (example shown in **Figure 3a**) of all the investigated samples (different mechanically activated powder mixtures) confirms mono-multi layered adsorption on the clear and stable powder surfaces with a morphology that suffered fragmentation and aggregation during the mechanical activation and is characterized by macropores or even limited number of the micropores [21]. According to the IUPAC classification, these adsorption–desorption isotherms belong to the aggregated particles that form slit-shaped
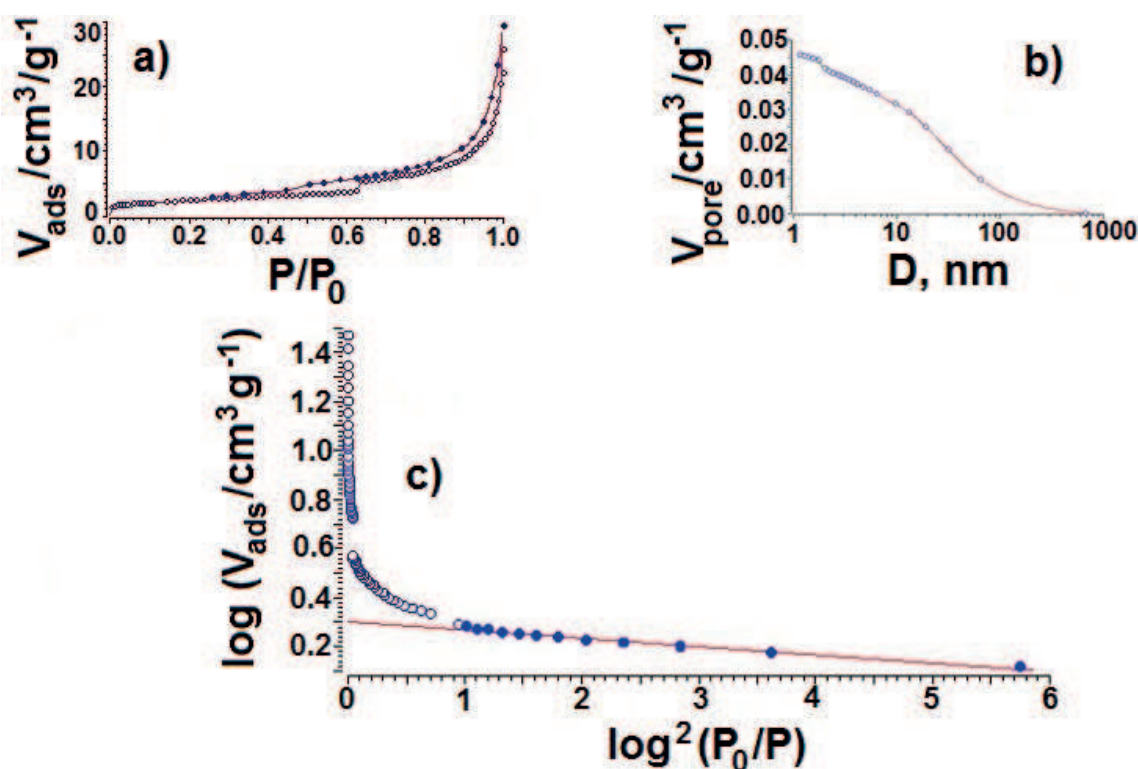
Figure 3. The nitrogen adsorption–desorption isotherm (a), the pore size distribution (b), and the pore volume distribution by Dubinin Radushevich line method (c), for the 10 min activated ZnO-SnO$_2$ powder mixture.

pores [22–24]. Isotherms have a reversible part (as physical adsorption is namely reverse) at the low relative pressures, when desorption is happening along the same isotherm path as adsorption, and hysteresis loops at higher relative pressures which happen because the desorption is harder when in very porous adsorbents, like in this material system, the condensation occurs inside fine pores and capillaries at lower than equilibrium pressure. The N_2 isotherm analysis (pore size distribution by Dollimore-Heal Poresizes [25] and Dubinin-Radushkevich Line [26] methods, an example shown in **Figure 3b** and **c**) gave the textural properties of the investigated different activated powder mixtures, and have shown that pores with the biggest total bulk volume were found in the powder mixture activated for 10 min, while lower total porosity (volume) was determined for the 40 min of activation, and the lowest for the other activation times (80 and 160 min) that had a smaller amount of the big pores (mesopores), like ZSO-40. The average mesopore diameters varied in the range from 22 nm (ZSO-10) to 79 nm (ZSO-80). The increase of the activation time, from 80 to 160 min, did not bring further texture-porosity evolution [21].

The second most important step in the ceramics processing is the consolidation of a mechanically activated power mixture by pressing. The microstructure of the sintered pellets (i.e. thermally treated consolidated powder mixtures) extremely depends on the quality of the green body (pressed mechanically activated powder mixture before the sintering process). It is very crucial to the whole technology of the ceramics production to establish the mathematical–physical correlation between the pressure of the compaction (consolidation), and the main macroscopic features of the investigated material (density or porosity), that is, to determine the compressibility of the investigated powders (dependence of the green body density vs. the compaction pressure). These compressibility investigations have actually a very practical nature, that is, to determine the pressing pressure needed for each of the investigated powder mixtures to obtain a specifically desired density. Different mechanochemically activated ZnO-SnO_2 powders were pressed under 49–392 MPa into 10 mm pellets. The green body density (green density) was determined for each of the samples by measuring the weight and dimensions of the obtained pellets with an error not bigger than 1% [27]. **Figure 4** shows the influence of the consolidation pressure vs. relative green density for differently activated powders from the ZnO-SnO_2 system.

The green densities of the nonactivated ZnO-SnO_2 powder mixture obtained under several applied pressures are significantly lower compared to the green densities of the 10, 40, 80 and 160 min activated ZnO-SnO_2 powder mixtures. The highest densities are obtained for the lowest activation time (10 min). Because the green densities of the 80 and 160 min activated powder mixtures have really close values, for clarity, the relative green densities of the 160 min activated powder mixture were left out in **Figure 4**. All dependency curves in **Figure 4** have the same shape, while their relationships point out to the general rule that the longtime of mechanical activation and the same applied compaction pressure results in a green density decrease. This is probably a consequence of the formation of a larger number of harder agglomerates (**Figure 2**) with prolonged activation and is actually a typical compressibility behavior of the powder materials. In other words, longer mechanical activation demands higher pressure force to obtain the green body with approximately same density. For the 80 min (and 160 min) activated ZnO-SnO_2 powder system, it is necessary to apply four times higher pressure than for 10 min
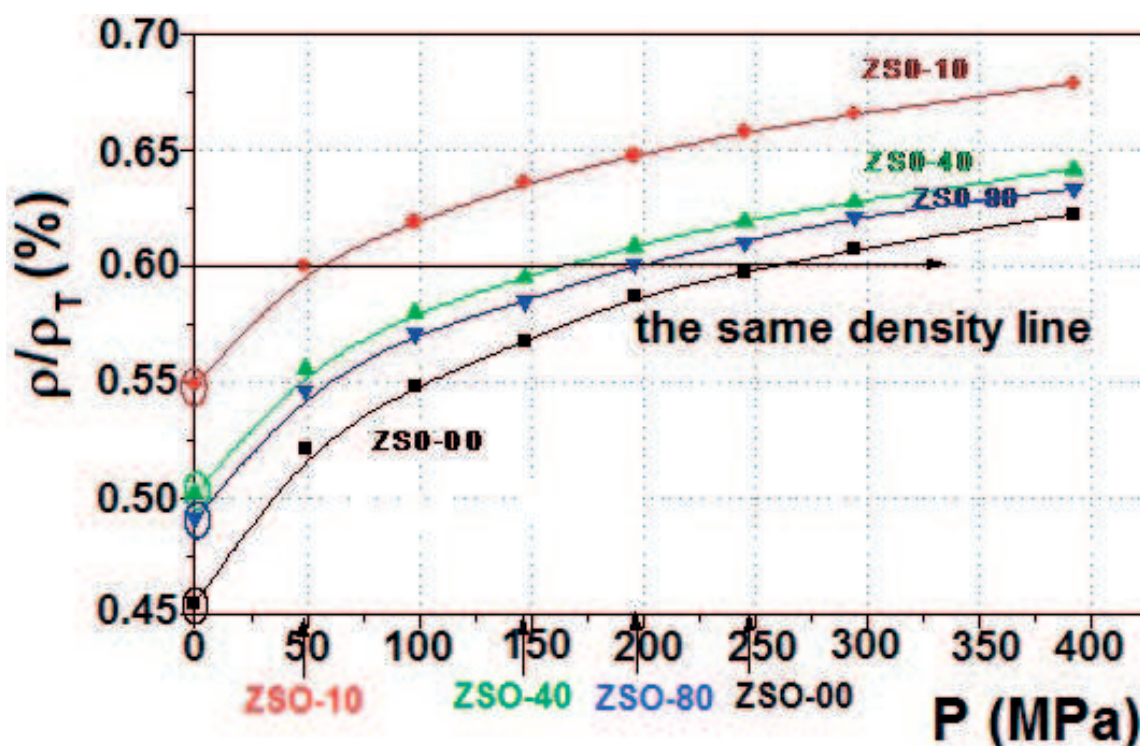
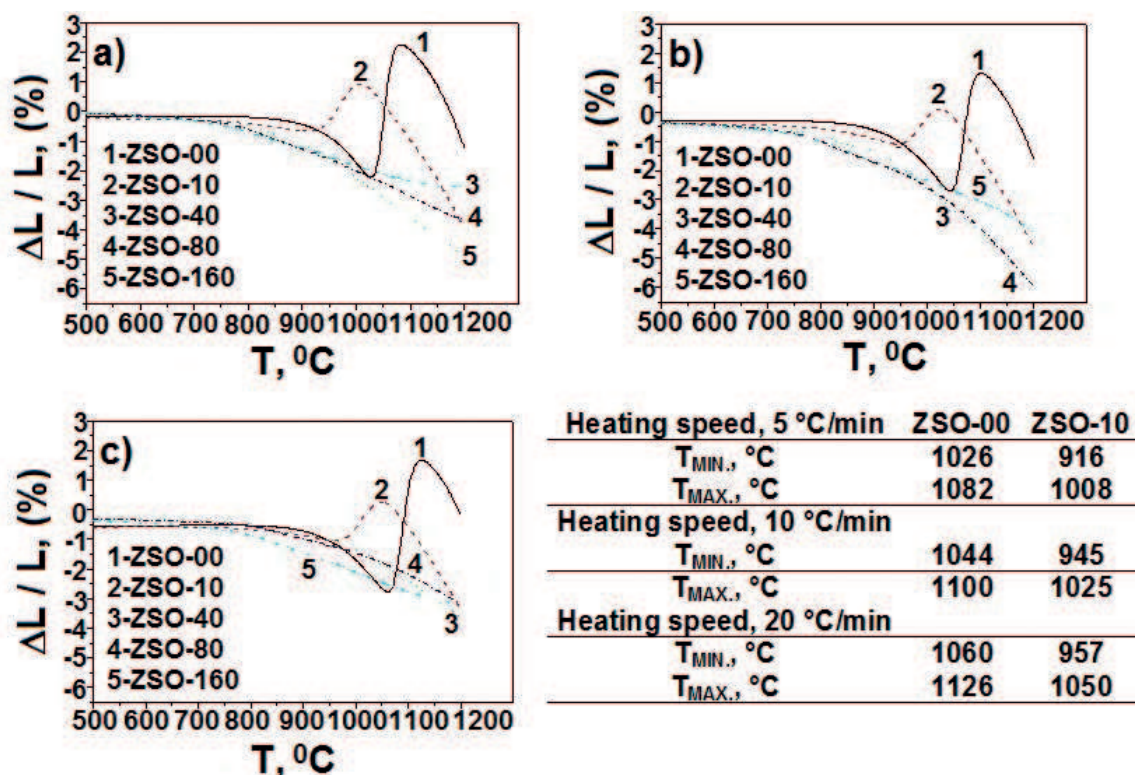**Figure 4.** The pressing pressure vs. green density for the ZnO-SnO$_2$ system [27].

activated powder mixture to have the green body with the same density. It is easy to spot on the so-called, "the same density line" in **Figure 4**, that shows the values of the pressure that have to be applied in order to obtain the green body that has the same density (60% of the theoretical density), no matter how activated ZnO-SnO$_2$ powder mixture is.

3. Mechanism and kinetics of sintering, and the porosity of consolidated ZnO-SnO$_2$ system

In order to investigate the influence of the mechanical activation on ZnO-SnO$_2$ systems densification, the green bodies of the different activated ZnO-SnO$_2$ powder mixtures were prepared by uniaxial pressing with different pressures (250, 50, 150, 200, 200 MPa was applied for ZSO-00, ZSO-10, ZSO-40, ZSO-80, and ZSO-160, respectively) in accordance with the findings in **Figure 4**, so the starting sintering density would be the same (3.769 g/cm^3) [27, 28] for all the investigated samples. Non-isothermal sintering kinetics was determined by monitoring the relative shrinkage of the green body by sensitive dilatometer, in the air up to 1200°C, with three different heating rates (5°C/min in **Figure 5a**, 10°C/min in **Figure 5b**, and 20°C/min in **Figure 5c**). All the results are shown in **Figure 5**.

The dilatometric results point to 800°C as the temperature when the densification process starts in ZSO-40, ZSO-80, and ZSO-160 samples. The dilatometric behavior of ZSO-00 and ZSO-10 is somehow different. The initial expansion in the ZSO-00 and ZSO-10 samples starts around 1000°C and continues in shrinkage. It is very important to determine the origin of this

Heating speed, 5 °C/min	ZSO-00	ZSO-10
$T_{MIN.}$, °C	1026	916
$T_{MAX.}$, °C	1082	1008
Heating speed, 10 °C/min		
$T_{MIN.}$, °C	1044	945
$T_{MAX.}$, °C	1100	1025
Heating speed, 20 °C/min		
$T_{MIN.}$, °C	1060	957
$T_{MAX.}$, °C	1126	1050

Figure 5. The dilatometric curves of differently activated ZnO-SnO_2 samples obtained by non-isothermal sintering in air, at different heating rates: (a) 5°C/min, (b) 10°C/min, and (c) 20°C/min, and up to 1200°C [28–30]. The inset table shows the minimum and maximum temperatures where the expansion and the shrinkage start, respectively, for the ZSO-00 and ZSO-10 samples.

deviation and its impact on the process of densification and further evolution of the material microstructure. This expansion cannot be explained just by the simple differences in the molar volumes of the samples because the theoretical density of zinc stannate spinel (6.42 g/cm³) is very close to the theoretical density of the equimolar mixture of ZnO and SnO_2 (6.24 g/cm³). Several mechanisms are described in the literature to explain phenomena like this, that is, the expansion of the powders during the solid-state reactions. In the oxide systems as ZnO-SnO_2, it is explained by to the separation of the particles when the reaction product is formed. The chemical reaction starts at 1026°C (when the heating speed is 5°C/min), 1044°C (when the heating speed is 10°C/min) and 1060°C (when the heating speed is 20°C/min) in the ZSO-00 sample, and at 916°C (heating speed, 5°C/min), 945°C (heating speed, 10°C/min) and 957°C (heating speed, 20°C/min) for the ZSO-10 sample (Inset Table in **Figure 5**). During the chemical reaction, the product, zinc stannate, causes the expansion of the ZSO-00 and ZSO-10 samples because the starting powder grains are being separated in the way that is illustrated in **Figure 6**.

The reaction sintering is a process during which the chemical reaction and the densification happen simultaneously. The temperature of the reaction sintering beginning is obviously lower for the longer mechanically activated ZnO-SnO_2 powder mixtures and higher when higher heating speeds were used during the thermal treatment. Some believe that the most important fact for the reaction sintering process is a defect degree of the formed microstructure during the chemical reaction. For the systems where the chemical reaction does not induce the
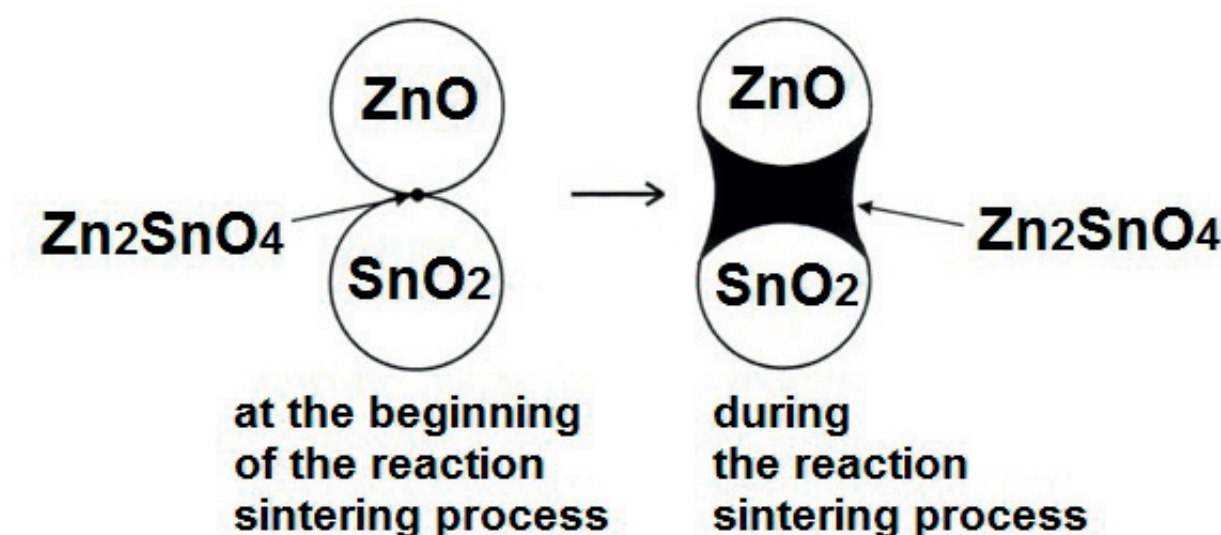
Figure 6. The schematic illustration of the solid-state reaction in the ZnO-SnO$_2$ system.

huge microstructure changes, obtaining higher densities and controlled grain growth does not depend on the fact whether the chemical reaction begins before or after the densification process. However, if the volume change during the reaction sintering is large, the densification should occur before the reaction if the high density and controlled grain growth are desired. The results obtained for ZSO-00 and ZSO-10 samples imply that the reaction between the ZnO and SnO$_2$ and formation of the Zn$_2$SnO$_4$ spinel in these samples begins before the process of sintering and it is accompanied by a very large expansion of the samples. In samples activated for 40 min and more, the shrinkage is dominant. The XRD results confirmed that in these samples zinc stannate spinel is a major phase so the process of densification prevails. The slope of the dilatometer curves of ZSO-40, ZSO-80, and ZSO-160 samples point to the possibility of the spinel phase formation in the shape of the agglomerates that progress by the increased activation time because the agglomeration inhibits the densification. The calculated green and sintered densities were 3.74 and 4.14 g/cm^3 (ZSO-40), 3.78 and 4.12 g/cm^3 (ZSO-80) and 3.79 and 3.86 g/cm^3 (ZSO-160), respectively. The densification is the highest for the sample activated for 40 min and the lowest for the longest activated sample (ZSO-160). The densities of all the samples increase during sintering but the highest value is obtained for the ZSO-40 sample. Hence, the relative shrinkage during sintering is primarily dependent on a distribution of the starting particles, their consolidation, and activity. The densities of all the sintered samples are lower than 70% of the theoretical density of zinc stannate. It is obvious that this structure is difficult to sinter. The porosity present in starting powder mixtures is preserved in the sintered samples as well. The starting powders are mainly made of the agglomerates, which are the reason why the packing of the particles during consolidation step is not ideal, and then it is so difficult to reach the high densification degree during sintering. This, together with the formation of the agglomerated spinel, is the main reason for the slow sintering process in this system. The moving force of the reaction sintering is the low free energy of the system as a result of the spinel phase formation through the diffusion mechanisms. The additional force is the high surface free energy induced by the process of mechanical activation of the starting powders, but only after the system gains the chemical balance.

The isothermal sintering was performed at 900 to 1200 °C (**Figure 7a**) for different time intervals (30–120 min) (**Figure 7b**). The relative densities were determined and used to calculate the obtained ceramics porosities (**Table 1**). The isothermal sintering is usually analyzed by investigating the shrinkage degree, which is described by the so-called Lanel parameter. This parameter connects the after sintering Π_S and starting porosity Π_0, that is, the green ρ_0, sintered ρ_S, and theoretical ρ_T density of the investigated material: $L = 1-(\Pi_S/\Pi_0) = (\rho_S - \rho_0)/(\rho_T - \rho_0)$. The joint structural characteristic of all the sintered samples is a large open porosity, ~40% and inhomogeneity which is a consequence of the powders "history" (the presence of the agglomerates and aggregates) (**Figure 2**), porosity in the starting powder mixtures and the solid-state reaction with the spinel formation (**Figure 6**). The formal sintering kinetic analysis by Lanel parameter (**Figure 8**) confirmed that mechanical activation of the starting powder mixtures influences the sinterability, but having all the results in mind, longer activation than 40 min is not necessary because the
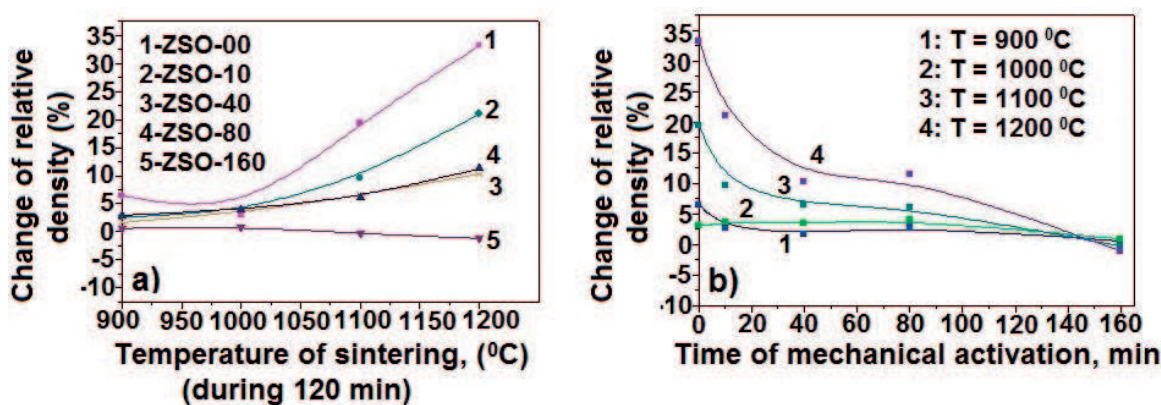
Figure 7. The change of the relative density vs. a) Temperature of the isothermal sintering and b) time of the mechanical activation, of the ZnO-SnO$_2$ system.

Sample	$\Pi_0 = 1-\rho_0/\rho_T$ (%)	$\Pi_S = 1-\rho_S/\rho_T$ (%)	Sample	$\Pi_0 = 1-\rho_0/\rho_T$ (%)	$\Pi_S = 1-\rho_S/\rho_T$ (%)
		$T_{SINTER.} = 900\ °C$			$T_{SINTER.} = 1100\ °C$
ZSO-00	48.6	45.3	ZSO-00	48.6	38.6
ZSO-10	41.9	46.4	ZSO-10	43.1	37.7
ZSO-40	45.3	44.4	ZSO-40	44.7	41.1
ZSO-80	45.8	44.2	ZSO-80	46.1	42.8
ZSO-160	46.4	46.1	ZSO-160	46.4	46.6
		$T_{SINTER.} = 1000\ °C$			$T_{SINTER.} = 1200\ °C$
ZSO-00	46.9	45.3	ZSO-00	48.4	31.3
ZSO-10	43.8	41.7	ZSO-10	42.8	30.8
ZSO-40	45.3	43.5	ZSO-40	45.3	39.7
ZSO-80	45.6	43.5	ZSO-80	46.4	40.3
ZSO-160	45.6	45.1	ZSO-160	46.6	47.2

Table 1. Porosity (%) for the green and isothermally sintered ZnO-SnO$_2$ samples.
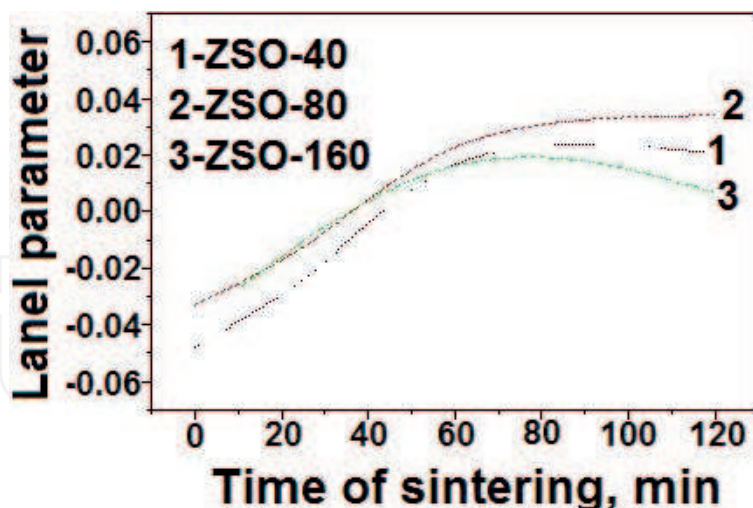
Figure 8. The Lanel parameter vs. time of sintering for the ZnO-SnO₂ samples activated 40, 80, and 160 min and sintered at 900°C for 2 hours.

effects of longer mechanical activation have a very little impact on the sinterability improvement. The mechanical activation longer than 40 min, on the other hand, is needed for more efficient zinc stannate synthesis.

The behavior of the differently activated samples of ZnO-SnO_2 system during the heat treatment was complemented with differential thermal analysis (DTA). From the shape of the exothermal peak of the nonactivated ZnO-SnO_2 powder mixture, it is obvious that starting from 400°C, the serious of exothermic, poorly separated changes (processes) occur. These processes lead to the formation of zinc stannate phase, which is confirmed by the XRD analysis [29, 30]. The exothermal effect in ZSO-10 is a consequence of the two processes: formation of the zinc stannate at lower temperatures and spinel crystal growth at higher temperatures.

The XRD analysis confirms the existence of the spinel peaks in ZSO-40, ZSO-80, and ZSO-160 samples, so the exothermal effect in these samples is only a result of the spinel growth during the thermal treatment [30]. With the higher activation times used in the preparation of the starting powder mixtures, the temperature of the exothermal peak is lowering (ZSO-00: 1135, ZSO-10: 1031, ZSO-40: 941, ZSO-80: 892, and ZSO-160: 849°C). The specific reaction enthalpy values were 1.69 (ZSO-10), 3.10 kJ/g (ZSO-40), and for the ZSO-80 and ZSO-160 samples, had the same value of 3.69 kJ/g, so the conclusion could be that the good condition for mechanochemical synthesis of the zinc stannate spinel is obtained already with 80 min of mechanical activation. The obtained results imply also the possibility of zinc stannate solid-state synthesis already at 900°C, which is a much lower temperature of Zn_2SnO_4 synthesis than previously found (1280°C) [31].

4. Morphology, optical and acoustic characterization of sintered ZnO-SnO₂ system

The influence of mechanical activation on the morphology, optical and thermal properties of the solid-state synthesized Zn_2SnO_4 was investigated by the scanning electron microscopy,

room temperature far infrared and photoacoustic spectroscopy [28, 32–34]. The reflectivity of near normal incidence light in the range between 100 and 1400 cm^{-1} as a function of the wave number showed the existence of eight ionic oscillators for all the investigated samples. The intensity of the reflectivity peaks was the highest for the sample activated for 10 min and gradually decreased with longer mechanical activation (40, 80 and 160 min, respectively). As confirmed by microstructural analysis longer times of activation lead to the increase of porosity and defects (**Figure 2**). The specificity of the obtained results is the two extra oscillators from the six that are expected to show for the known Wyckoff sites for zinc stannate structure and calculated by nuclear site group analysis, which is obviously the result of mechanical activation and sintering [32, 33]. It is known that the mechanical activation is responsible for the formation of the defects and after sintering a structure that contains pores, aggregates and intergranular material besides crystalline grains [32] (**Figure 9a–d**). As shown previously, the activation of 10 min brings the significant refinement in the crystallite size of the initial oxides, while the beginning of the spinel zinc stannate phase formation starts after 40 min of activation [21, 30]. The agglomeration and high porosity is a feature of all the mechanically activated samples, and it increases with the longer activation times and remains also after the sintering process (**Figure 9**). The ceramic materials with a large open porosity like zinc stannate obtained by the reaction sintering processing described in this review paper are convenient for the application in the humidity sensors. Atmospheric water can be absorbed on the grain surfaces inside pores or condensed in the small channels and pores [28]. Humidity sensor has to have features like high sensitivity, reversibility, fast response, the broad range of moisture selectivity, chemical, and thermal stability, which depends on the microstructure formed
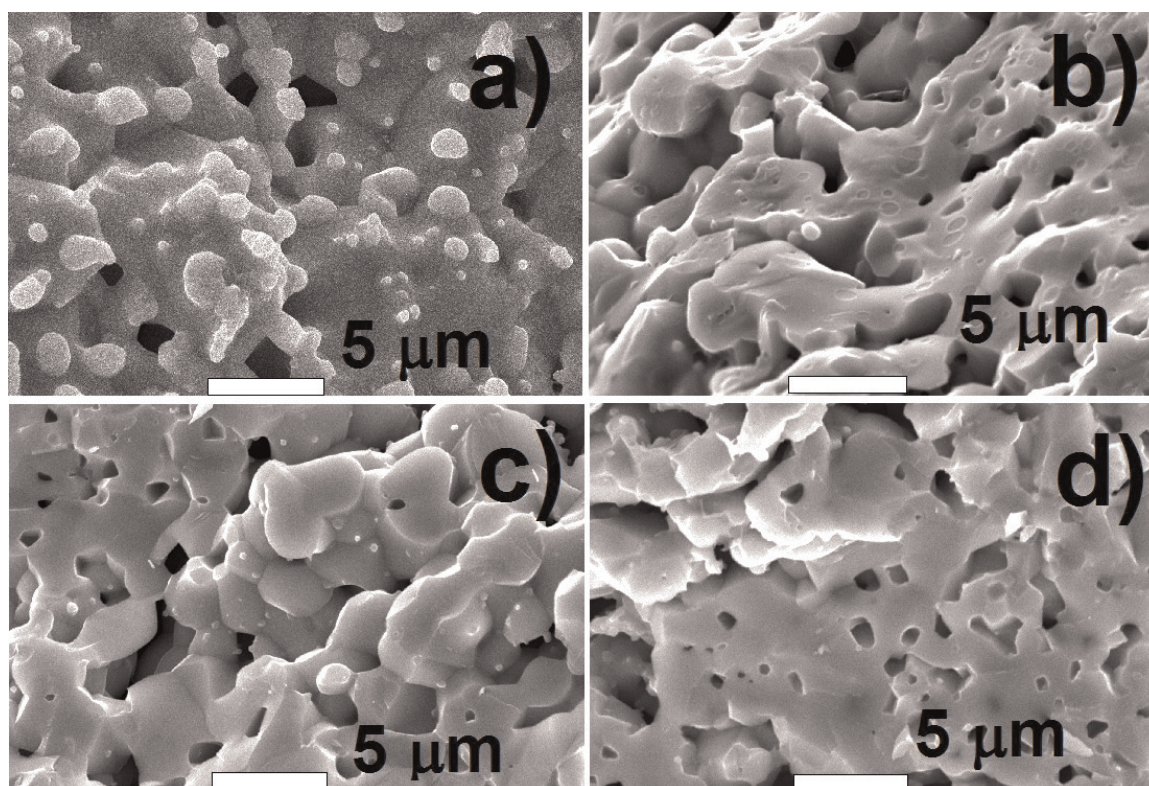
Figure 9. SEM micrographs of ZnO-SnO$_2$ ceramics prepared by mechanical activation for, (a) 10, (b) 40, (c) 80 and (d) 160 min and isothermal sintering at 1300°C for 2 hours.

during the synthesis procedure. The thermal characterization of these materials is very important. Photoacoustic spectroscopy was used to determine the thermal and transport properties of 40, 80, and 160 min activated and non-isothermally sintered up to 1200°C samples (heating rate of 5°C/min) [28] and the 10, 40, 80 and 160 min activated and isothermally sintered at 1300°C for 2 hours samples [34]. The experimental photoacoustic phase and amplitude spectra were recorded as a function of the chopped frequency of the laser beam (red laser with power of 25 mW, λ = 632 nm) in a thermal-transmission detection configuration and analyzed by theoretical Rosencwaig-Gersho thermal-piston model [35], which enable determination of the materials thermal properties including thermal diffusivity, diffusion coefficient of the minority free carriers and optical absorption coefficient.

The differences in thermal-electrical characteristics that were obtained again indicated that the changes in the material are induced by the differences in the processing routes of the powders before sintering. With the increase of the activation time and the formation of a single phase zinc stannate the thermal diffusivity value increases. The thermal diffusivity of zinc stannate material obtained by non-isothermal sintering route (0.21×10^{-7}, 1.80×10^{-7} , and 10.06×10^{-7} m^2 s^{-1}, for the ZSO-40, ZSO-80, and ZSO-160 samples, respectively) are to our best knowledge the first time ever measured values of this kind [28]. The photoacoustic analysis for differently activated and isothermally sintered ceramic samples shown differences in photoacoustic spectra, especially specific are the results obtained for the ZSO-10 sample. The frequency dependence photoacoustic phase has an explicit minimum for the samples prepared with higher activation times [34]. In the amplitude diagrams, at critical frequencies where phase diagram has the explicit minimum, a knee like a change of the curve rate occurs. It is obvious that at those frequencies in the samples activated longer than 10 min, the significant changes in the material properties appear. Those samples act as thermally thick at frequencies higher than the critical, and thermally thin at the frequencies lower than critical. In the area of lower frequencies, the dominant role in the generation of the photoacoustic signal has the thermal diffusivity and optical absorption coefficient. In the frequency range when the samples are thermally thick, the intensity and phase of the photoacoustic signal depend primarily upon the electrical transport properties of the investigated samples. The increase in the thermal diffusivity value with the increase of the activation time is confirmed in these samples as well which again points to the fact that higher activation times are responsible for the formation of porous, defect and low-density microstructure. This confirms, once more, that the grain growth of the spinel phase slows down the densification process, and together with the agglomerates formed during the mechanical activation, causes the appearance of a highly porous microstructure [34].

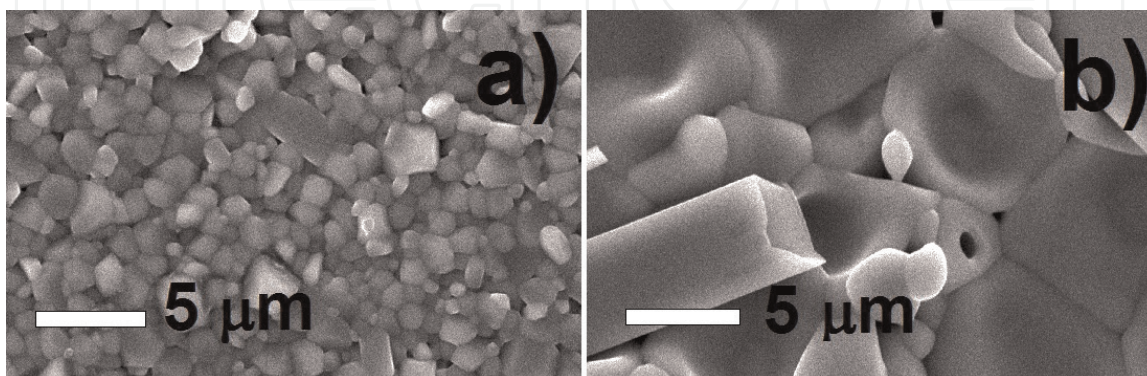## 5. Liquid phase sintering of the ZnO-SnO$_2$ system

The effect of small amounts of bismuth oxide (Bi$_2$O$_3$) on the microstructure, optical, structural and electrical properties of the spinel-type ZnO-SnO$_2$ (zinc-tin-oxide) ceramics was investigated [36–39] to complement the above-shown research on the zinc-tin-oxide porous ceramics. Two series of samples were made for this purpose. Samples of the first series were used as the reference and were prepared by mechanical activation in different time intervals (10, 40, 80,

and 160 min), pressing under 980 MPa in 10 mm diameter pellets, and isothermal sintering at 1300°C, for 2 hours. They were used for selecting the optimal conditions for the preparation of Bi-doped $ZnO-SnO_2$ samples (the second series samples). The infrared spectra of the first series samples were used also as the reference spectra to compare with infrared spectra's of samples of the second series. XRD analysis of the first series samples confirmed the presence of only Zn_2SnO_4 spinel phase [36, 37]. The density measurements, however, show that the slightly higher density was obtained for the starting powder mixture activated for 10 min (**Table 2**). Comparing the obtained relative densities of the sintered samples at temperatures from 900 to 1200°C (**Table 1**, where the values were in the range from 52.8–69.2%), and the ones in **Table 2**, it is easy to conclude that by increasing the sintering temperature the relative density of the $ZnO-SnO_2$ ceramic material is increased. Because of the slightly higher densities obtain for the 10 min activated sample; this parameter of synthesis (10 min of activation) was applied in the preparation of the samples from the second series. Samples of the second series were then prepared with the same starting powder mixtures, with the molar ratio of $ZnO:SnO_2 = 2:1$, but with the addition of 0.5, 1.0 and 1.5 mol.% of Bi_2O_3 (samples marked as ZSO-0.5, ZSO-1, and ZSO-1.5, respectively), mechanical activation for 10 min, pressing under 980 MPa and isothermal sintering at 1300°C for 2 hours. The highest relative density was obtained for the 1.0 mol.% of Bi_2O_3 (~92%) (**Figure 10a**), while the increasing concentration of Bi_2O_3 in the system (1.5 mol.%) lead to the decrease of the relative density (~87) probably because of the further grain growth and problematic packing of the bigger particles that are now more present in the system (**Figure 10b**). These conclusions are confirmed by the scanning electron microscopy measurements shown in **Figure 10**.

| Samples of the first series	ρ_S/ρ_T (%)	Samples of the second series	ρ_0 (g/cm³)	ρ_0/ρ_T (%)	ρ_S (g/cm³)	ρ_S/ρ_T (%)
ZSO-10	75.9	ZSO	3.92	62.96	5.25	84.44
ZSO-40	75.7	ZSO-0.5	4.12	65.79	5.63	89.93
ZSO-80	75.5	ZSO-1.0	4.12	65.19	5.81	92.21
ZSO-160	75.3	ZSO-1.5	4.22	66.51	5.49	86.58

Table 2. The sintered relative densities of the samples from the first series, and relative densities before and after the sintering for the Bi_2O_3 doped $ZnO-SnO_2$ samples.

Figure 10. SEM micrographs of (a) 1 and (b) 1.5 mol.% Bi_2O_3 doped $ZnO-SnO_2$ ceramics.

Addition of the small amounts of Bi_2O_3 to the ZnO-SnO_2 system creates conditions for the liquid phase sintering and enhances the densification process. The obtained structure and morphology was examined using XRD and SEM-EDS [36–39]. FTIR and impedance spectroscopy were used to investigate the optical and electrical properties [38, 39]. Bi_2O_3 doping creates the conditions for the liquid phase sintering. Bismuth oxide forms $Bi_2Sn_2O_7$ pyrochlore phase with SnO_2 and in the presence of ZnO leads to the formation of Zn_2SnO_4 spinel and Bi_2O_3 liquid phase between 1000 and 1100°C, according to the following reaction [36]: $Bi_2Sn_2O_7 + 4ZnO \rightarrow 2Zn_2SnO_4 + Bi_2O_3(l)$. This brings a new dynamic into the ZnO-SnO_2 sintering mechanism. The base system mixture ($2ZnO$-SnO_2) grains are completely surrounded by the thin film of liquid Bi_2O_3, which directly influence the densification, grain growth and the solid-state reaction between the ZnO and SnO_2. No XRD proof of Bi_2O_3 was found in the sintered samples, either because the amount of Bi_2O_3 was under the XRD detection limit, or such high temperature of sintering (1300°C) caused the Bi_2O_3 to evaporate (evaporation of Bi_2O_3 starts at 825°C) [37]. The addition of Bi_2O_3 stimulates the ion substitution between Sn^{4+} and Zn^{2+} which results in ZnO/SnO_2 solid solution formation with rather limited regions of pure Zn_2SnO_4 [36, 38] (**Figure 11**). Probably the diffusion-evaporation mechanisms are responsible for the reaction between the ZnO and SnO_2 in this case of this material sintered at such high temperatures, and not just the ordinary diffusion processes that happen in the usual solid-state chemical reactions. A limited evaporation of ZnO is also inevitable [37]. The ZnO evaporation opens up larger pores in places where the SnO_2 was not available for the reaction due to the incomplete mixing. The zinc oxide condenses unreacted on the walls of the cavities upon cooling. The residual SnO_2 appears to balance the evaporated ZnO. As said previously, the Zn_2SnO_4 has a cubic inverse spinel (AB_2O_4) structure so the A and B sites can substitute for each other during sintering based on the following reaction: $AB_2O_4 \rightarrow (AB) BO_4$. Even though the valance of the Sn^{4+} is higher than of the Zn^{2+} ion the substitution is mutual [38] and according to the obtained results [36–39] the Bi-doping strongly promoted this substitution and contribute to the Zn_2SnO_4-SnO_2 solid solution formation, along with the larger regions of pure spinel Zn_2SnO_4 (**Figure 11**) and smaller areas of residual SnO_2. In Bi-doped ZnO-SnO_2 system, the liquid phase assisted sintering mechanism is obviously responsible for these dramatic microstructural changes and the deviation from the expected formation of single phase cubic spinel Zn_2SnO_4. The enhancement of the densification process and higher bulk
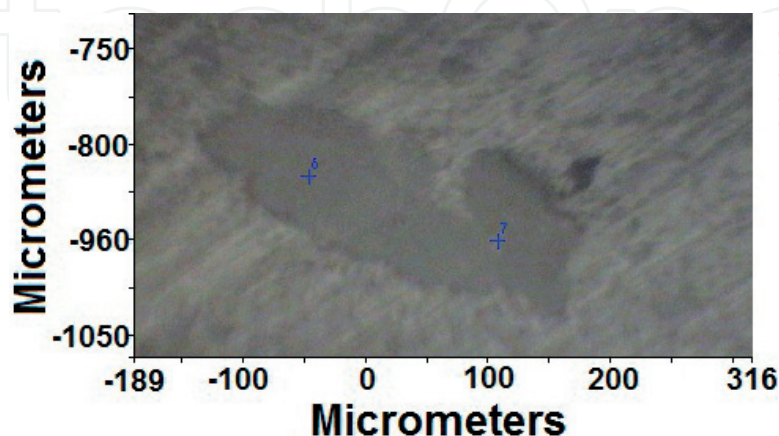
Figure 11. The ZSO-1 sample image taken with an optical microscope. The dark-gray area belongs to the pure Zn_2SnO_4 phase and it is surrounded by the "matrix" region composed of Zn_2SnO_4-SnO_2 solid solution (noticeable recording points 6 and 7, marks the positions where the additional IR and EDS analysis were performed and shown elsewhere [36, 38]).

relative densities are expected. The influence of the addition of Bi_2O_3 on the densification process was investigated by monitoring the change in the relative density vs. the molar percentage of the Bi_2O_3 added, and it shows an increase in relative density of sintered samples (~ 92%) with the addition of Bi_2O_3 up to 1.0 mol%, while further addition of 1, 5 mol% Bi_2O_3 leads to a decrease in relative density (~ 87%) [37]. This is probably due to further grains growth and packaging problem of much larger particles. The general conclusion is that the optimal amount of Bi_2O_3 under applied sintering conditions (1300°C, 2 hours) for achieving the best possible densification is 1.0 mol%.

The agglomeration and high porosity present in the starting mixtures are also retained in the sintered samples (porosity ~25%) (**Table 2**). The general microstructure of the sintered samples of the second series is characterized by the denser sintered areas compared to the reference sample (**Figures 9** and **10**). The "matrix" consists more of the non-stoichiometric zinc stannate, $Zn_{2-x}Sn_{1+x}O_4$ and represent some kind of a solid-solution, where dark-gray regions are closer to the composition of pure Zn_2SnO_4, while smaller areas are composed of the residual SnO_2 whose polygonal grains are like inserted into the spinal structure (**Figure 10b**) [36–38].

The Bi-addition to the ZnO-SnO_2 system reflected on its optical properties as well. Although, the FTIR spectra [38] were similar to the previously obtained for Zn_2SnO_4 spinel [30, 32, 33] and were characterized by two extra oscillators (eight in total) attributed to the cation disorder in the crystal lattice induced by preparation procedure, compared to the six predicted by group theory analysis that belongs to the zinc stannate structure, it showed also the additional three more peaks that belong to SnO_2 phase (ω_{TO}) found at 244 and 288 cm^{-1}, and the most intensive bulk mode of SnO_2 at 613 cm^{-1}, which position was shifted to higher frequency in ZSO-1 sample [36, 38].

The impedance spectroscopy measurements provided evidence of the intrinsic features of the grain-boundary phenomenon in this kind of ceramic material and point to its possible application in the nonohmic devices [39]. Impedance diagrams of SnO_2-Zn_2SnO_4 ceramics showed Cole-Cole type behavior, where complex impedance data resulted in the semi-circles with the high degree of overlapping which is consistent with the reported semiconductor properties of this kind of ceramic material.

6. Summary

The optimal conditions for the best zinc stannate synthesis by reaction sintering of the mechanically activated ZnO and SnO_2 powder mixtures in a high-energy planetary ball mill, in the time intervals from 0 to 160 min, were obtained. The mechanochemical activation of 40 min and more creates the conditions for the beginning of the Zn_2SnO_4 formation. The pure stannate phase was obtained in the sample activated for 160 min and sintered at 1200 °C and higher. A joint structural feature of all the polycrystalline sintered bulk samples is a large open porosity. Formal analysis of the sintering kinetics using Lanel parameter confirmed that mechanical activation affects the sinterability only for the activation less than 40 min, while longer milling intervals have no more effect on the obtained Zn_2SnO_4 large porosity. In the materials characterization, it was shown that thermal diffusivity increases with the activation

time and progression of the zinc stannate formation. SEM and FTIR results agree well in the conclusion that longer times of mechanical activation lead to increased porosity and defects. The FTIR spectra were numerically analyzed and oscillator parameters were calculated. Two more oscillators were observed compared to six predicted by the group theory for the single crystal Zn_2SnO_4, as a result of the synthesis procedure. The obtained defect structure of the Bi-doped ZnO-SnO_2 system is a direct consequence of the structural changes in all the hierarchy levels induced by the liquid phase sintering mechanism, which strongly influences the optical and electrical properties of the obtained material as well. By selecting the conditions and the ways of the sample preparation during the process of mechanical activation and sintering, it is possible to alter the microstructure, phase composition, optical and electrical properties of the resulting zinc-tin-oxide ceramics to fit the best the desired applications.

Acknowledgements

Author details

Tamara Ivetić

Address all correspondence to: tamara.ivetic@df.uns.ac.rs

University of Novi Sad, Faculty of Sciences, Department of Physics, Trg Dositeja Obradovića, Novi Sad, Serbia

References

[1]   Peiteado M, Iglesias Y, Fernández JF, De Frutos J, Caballero AC. Microstructural development of tin-doped ZnO bulk ceramics. Materials Chemistry and Physics. 2007;**101**:1-6

[2]   Šepelák V, Becker SM, Bergmann I, Indris S, Scheuermann M, Feldhoff A, Kübel C, Bruns M, Stürzl N, Ulrizh AS, Ghafari M, Hahn H, Grey CP, Becker KD, Heitjans P. Nonequilibrium structure of Zn_2SnO_4 spinel nanoparticles. Journal of Materials Chemistry. 2012;**22**:3117-3126

[3]   Baruah S, Dutta J. Zinc stannate nanostructures: Hydrothermal synthesis. Science and Technology of Advanced Materials. 2011;**12**:013004 (18pp)

[4]   Yuan H-L, Li J-C. Effect of annealing temperature on the growth of Zn-Sn-O nanocomposite thin films. Journal of Alloys and Compounds. 2017;**714**:114-119

[5]   Salohub AO, Voznyi AA, Klymov OV, Safryuk NV, Kurbatov DI, Opanasyuk AS. Determination of fundamental optical constants of Zn_2SnO_4 films. Semiconductor Physics, Quantum Electronics & Optoelectronics. 2017;**20**:79-84

[6] Ivetić T, Nikolić MV, Young DL, Vasiljević-Radović D, Urošević D. Photoacousic and optical properties of zinc-stannate thin films. Materials Science Forum. 2006;**518**:465-470

[7] Liu X, Niu C, Meng J, Xu X, Wang X, Wen B, Guo R, Mai L. Gradient-temperature hydrothermal fabrication of hierarchical Zn_2SnO_4 hollow boxes stimulated by thermodynamic phase transformation. Journal of Materials Chemistry A. 2016;**4**:14095-14100

[8] Lehnen T, Zopes D, Mathur S. Phase-selective microwave synthesis and inkjet printing applications of Zn_2SnO_4 (ZTO) quantum dots. Journal of Materials Chemistry. 2012;**22**:17732-17736

[9] Young DL, Williamson DL, Coutts TJ. Structural characterization of zinc stannate thin films. Journal of Applied Physics. 2002;**91**:1464-1471

[10] Young DL, Moutinho H, Yan Y, Coutts TJ. Growth and characterization of radio frequency magnetron sputter-deposited zinc stannate, Zn_2SnO_4, thin films. Journal of Applied Physics. 2002;**92**:310-319

[11] Rong A, Gao XP, Li GR, Yan TY, Zhu HY, Qu JQ, Song DY. Hydrothermal synthesis of Zn_2SnO_4 as anode materials for Li-ion battery. The Journal of Physical Chemistry. B. 2006;**110**:14754-14760

[12] Alpuche-Aviles MA, Wu Y. Photoelectrochemical study of the band structure of Zn_2SnO_4 prepared by the hydrothermal method. Journal of the American Chemical Society. 2009;**131**:3216-3224

[13] Fu X, Wang X, Long J, Ding Z, Yan T, Zhang G, Zhang Z, Lin H, Fu X. Hydrothermal synthesis, characterization, and photocatalytic properties of Zn_2SnO_4. Journal of Solid State Chemistry. 2009;**182**:517-524

[14] Lana-Villarreal T, Boschloo G, Hagfeldt A. Nanostructured zinc stannate as semiconductor working electrodes for dye-sensitized solar cells. Journal of Physical Chemistry C. 2007;**11**:5549-5556

[15] Wang X, Wang Y-F, Luo Q-P, Ren J-H, Li D-J, Li X-F. Highly uniform hierarchical Zn_2SnO_4 microspheres for the construction of high performance dyesensitized solar cells. RSC Advances. 2017;**7**:43403-43409

[16] Li Y, Pang A, Zheng X, Wei M. CdS quantum-dot-sensitized Zn_2SnO_4 solar cell. Electrochimica Acta. 2011;**56**:4902-4906

[17] Stambolova I, Konstantinov K, Kovacheva D, Peshev P, Donchev T. Spray pyrolysis preparation and humidity sensing characteristics of spinel zinc stannate thin films. Journal of Solid State Chemistry. 1997;**128**:305-309

[18] Jiang Y-Q, Chen X-X, Sun R, Xiong Z, Zheng L-S. Hydrothermal synthesis and gas sensing properties of cubic and quasi-cubic Zn_2SnO_4. Materials Chemistry and Physics. 2011;**129**:53-61

[19] Yang HM, Ma SY, Yang GJ, Chena Q, Zeng QZ, Ge Q, Ma L, Tie Y. Synthesis of La_2O_3 doped Zn_2SnO_4 hollow fibers by electrospinning method and application in detecting of acetone. Applied Surface Science. 2017;**425**:585-593

[20] Movahedi M, Hosseinian A, Bakhshaei M, Rahimi M, Arshadnia I. Micro-spherical SnO_2/Zn_2SnO_4: Synthesis, heat treatment and photocatalytic efficiency for decolorization of two dye mixture in wastewater. Journal of Applied Chemistry. 2017;**11**:11-16

[21] Ivetić T, Vuković Z, Nikolić MV, Pavlović VB, Nikolić JR, Minić D, Ristić MM. Morphology investigation of mechanically activated ZnO-SnO_2 system. Ceramics International. 2008;**34**:639-643

[22] Gregg SH, Sing KS. Adsorption, Surface Area and Porosity. New York: Academic Press; 1967

[23] Rouquerol F, Rouquerol J, Sing K. Adsorption by Powders and Porous Solids. London: Academic Press; 1999

[24] Sing KS, Everett DH, Haul RAW, Moscou L, Pierotti RA, Rouguero J, Siemieniewska T. Reporting physisortion properties data for gas/solid systems with special reference to the determination of surface area and porosity. Pure and Applied Chemistry. 1985;**57**:603-619

[25] Dollimore D, Heal GR. An improved method for the calculation of pore size distribution from adsorption data. Journal of Applied Chemistry. 1964;**14**:109-114

[26] Dubinin MM. Physical adsorption of gases and vapors in microspores. In: Cadenhead DA, editor. Progress in Surface and Membrane Science. New York: Academic Press; 1975. pp. 1-70

[27] Ivetić TB, Vojisavljević KM, Srećković T. Influence of mechanical activation on consolidation of ZnO-SnO_2 powder system, Fundamental problems of Physics and Technology of Materials, Proceedings of Scientific Meeting Physics and Technology of Materials-FITEM'04, 12-15 October 2004, Čačak, Serbia, p. 115-121. (In Serbian)

[28] Ivetić T, Nikolić MV, Nikolić PM, Blagojević V, Đurić S, Srećković T, Ristić MM. Investigation of zinc stannate synthesis using photoacoustic spectroscopy. Science of Sintering. 2007;**39**:153-160

[29] Nikolic N, Marinkovic Z, Sreckovic T. The influence of grinding conditions on the mechanochemical synthesis of zinc stannate. Journal of Materials Science. 2004;**39**:5239-5242

[30] Ivetić T. Synthesis and characterization of the zinc stannate spinel, M. Sc Thesis. Serbia: University of Belgrade, Faculty of Physical Chemistry; 2006 (In Serbian)

[31] Hashemi T, Al-Allak HM, Illingsworth J, Brinkman AW, Woods J. Sintering behaviour of zinc stannate. Journal of Materials Science Letters. 1990;**9**:776-778

[32] Nikolić MV, Ivetić T, Paraskevopoulos KM, Zorbas KT, Blagojević V, Vasiljević-Radović D. Far infrared reflection spectroscopy of Zn_2SnO_4 ceramics obtained by sintering mechanically activated ZnO-SnO_2 powder mixtures. Journal of the European Ceramic Society. 2007;**27**:3727-3730

[33] Nikolić MV, Ivetić T, Young DL, Paraskevopoulos KM, Zorba TT, Blagojević V, Nikolić PM, Vasiljević-Radović D, Ristić MM. Far infrared properties of bulk sintered and thin film Zn_2SnO_4. Materials Science and Engineering B. 2007;**138**:7-11

[34] Ivetić TB, Nikolić MVP, Pavlović VB, Nikolić PM, Ristić MM. Photoacoustic spectroscopy investigation of sintered zinc-tin-oxide ceramics. Hemijska industrija. 2007;**61**:142-146 (In Serbian)

[35] Rosencwaig A, Gersho A. Theory of the photoacoustic effect with solids. Journal of Applied Physics. 1976;**47**:67-69

[36] Ivetić T. Influence of Bi_2O_3 on the sintering of ZnO-SnO_2 ceramics, Ph.D. Thesis. Serbia: University of Belgrade, Faculty of Physical Chemistry; 2008. (in Serbian)

[37] Ivetić T, Nikolić MV, Slankamenac M, Živanov M, Minić D, Nikolić PM, Ristić MM. Influence of Bi_2O_3 on microstructure and electrical properties of ZnO-SnO_2 ceramics. Science of Sintering. 2007;**39**:229-240

[38] Ivetić T, Nikolić MV, Paraskevopoulos KM, Pavlidou E, Zorba TT, Nikolić PM, Ristić MM. Combined FTIR and SEM-EDS study of Bi_2O_3 doped ZnO-SnO_2 ceramics. Journal of Microscopy (Oxford). 2008;**232**:498-503

[39] Slankamenac M, Ivetić T, Nikolić MV, Ivetić N, Živanov M, Pavlović VB. Impedance response and dielectric relaxation in liquid-phase sintered Zn_2SnO_4-SnO_2 ceramics. Journal of Electronic Materials. 2010;**39**:447-455